Kinetics and Mechanisms of MOCVD Processes for the Fabrication of Sr-Containing Films From $Sr(hfac)_2$Tetraglyme Precursor

Guglielmo G. Condorelli, Annalisa Baeri, and Ignazio L. Fragalà*

Dipartimento di Scienze Chimiche, Università di Catania and INSTM udr di Catania, V.le Andrea Doria 6, 95125 Catania, Italy

Received April 22, 2002. Revised Manuscript Received August 13, 2002

The MOCVD process of $Sr(hfac)_2$ tetraglyme has been studied in horizontal, low-pressure hot wall and cold wall reactors under various experimental conditions. In all the investigated conditions, the deposition process results in the formation of polycrystalline SrF_2 films. The kinetics and the mechanism of film growth have been investigated by combining "in situ" FTIR techniques and "ex situ" techniques for chemical and structural analyses (energy-dispersive X-ray microanalysis, X-ray photoelectron spectroscopy, and X-ray diffraction). Two different reaction pathways have been proposed depending on deposition temperature. At low temperature a heterogeneous mechanism based on precursor adsorption, followed by the demolition of the β-diketonate framework, has been suggested; at high temperature, a homogeneous decomposition in which the fluorine transfer to the Sr atom leads to SrF_2, CF_2O, and acylketenes can occur.

Introduction

Strontium-based materials in the form of thin films are currently attracting growing interest in several strategic areas. Thus, transparent Sr-containing fluoride glasses (such as $SrAlF_5$) have a key role for optical coatings and luminescent devices[1−5] and strontium titanates are of interest for their applications as high-K materials in DRAMs,[6−17] while Ln-doped Sr sulfide[18] and Bi−Sr−Ca−Cu mixed oxides[19] are efficient materials for electroluminescent devices and superconducting electronics, respectively. Particular attention has recently been devoted also to $SrBi_2Ta_2O_9$ (SBT) ferroelectric oxides due to the great potentiality for ferroelectric nonvolatile random access memories (FeRAM).[20−25] SBT films can be fabricated through several techniques including pulsed laser deposition,[26,27] sol−gel,[28,29] metal−organic deposition,[30−34] and metal−organic chemical vapor deposition (MOCVD).[35−43] Among them, MOCVD appears the most viable route for the semiconductor industry because of the superior step coverage compared to that of other deposition techniques.

(1) Purdy, A. P.; Berry, A. D.; Holm, R. T.; Fatemi, M.; Gaskill, D. K. *Inorg. Chem.* **1989**, *28*, 2799.
(2) Kuck, S.; Sokolska, I. *J. Electrochem. Soc.* **2002**, *149*, J27.
(3) Gutierrez, R. E.; Rodriguez, F.; Moreno, M.; Alcala, R. *Radiat. Eff. Defects Solids* **2001**, *154*, 287.
(4) Fujihara, S.; Ono, S.; Kishiki, Y.; Tada, M.; Rimura, T. *J. Fluorine Chem.* **2000**, *105*, 65.
(5) Ronchin, S.; Rolli, R.; Montagna, M.; Duverger, C.; Tikhomirov, V.; Jha, A.; Ferrari, M.; Righini, G. C.; Pelli, S.; Fossi, M. *J. Non-Cryst. Solids* **2001**, *284*, 243.
(6) Kirchoefer, S. W.; Cukauskas, E. J.; Barker, N. S.; Newman, H. S.; Chang, W. *Appl. Phys. Lett.* **2002**, *80*, 1255.
(7) Nagel, N.; Costrini, G.; Lian, J.; Athavale, S.; Economikos, L.; Baniecki, J.; Wise, M. *Integr. Ferroelectr.* **2001**, *38*, 259.
(8) Samantaray, C. B.; Dhar, A.; Mukherjee, M. L.; Bhattacharya, D.; Ray, S. K. *Mater. Sci. Eng. B* **2002**, *B88*, 14.
(9) Li, T.; Hsu, S. T. *J. Phys. IV* **2001**, *11*, Pr3/1139.
(10) Fitsilis, F.; Regnery, S.; Ehrhart, P.; Waser, R.; Schienle, F.; Schumacher, M.; Dauelsberg, M.; Strzyzewski, P.; Juergensen, H *J. Eur. Ceram. Soc.* **2001**, *21*, 1547.
(11) Min, Y.-S.; Cho, Y. J.; Kim, D.; Lee, J.-H.; Kim, B. M.; Lim, S. K.; Lee, I. M.; Lee, W. I. *Chem. Vap. Deposition* **2001**, *7*, 146.
(12) Lee, J.-H.; Rhee, S.-W. *J. Electrochem. Soc.* **2001**, *148*, C409.
(13) Yamamuka, M.; Kawahara, T.; Tarutani, M.; Horikawa, T.; Shibano, T.; Oomori, T. *Jpn. J. Appl. Phys., Part 1* **2001**, *40*, 3435.
(14) Park, J.; Hwang, C. S.; Yang, D. Y. *J. Mater. Res.* **2001**, *16*, 1363.
(15) Kil, D.-S.; Park, J.-B.; Lee, J.-S.; Yoon, J.-W.; Yu, Y.-S.; Roh, J.-S.; Kim, C.-T.; Hwang, J.-M. *Integr. Ferroelectr.* **2001**, *33*, 291.
(16) Yoo, D. C.; Lee, J. Y. *Mater. Lett.* **2001**, *47*, 258.
(17) Baumann, P. K.; Kaufman, D. Y.; Im, J.; Auciello, O.; Streiffer, S. K.; Erck, R. A.; Giumarra, J. *Integr. Ferroelectr.* **2001**, *34*, 255.
(18) Heikkinen, H.; Johansson, L.-S.; Nykanen, E.; Niinisto, L. *Appl. Surf. Sci.* **1998**, *133*, 205.
(19) Yonemitsu, K.; Inagaki, K.; Ishibashi, T.; Kim, S.; Lee, K.; Sato, K. *Physica C* **2002**, *367*, 414.
(20) Ramesh, P.; Aggarwal, S.; Augello O. *Mater. Sci. Eng. B* **2001** 32.
(21) Park, J. D.; Oh, T. S. *Integr. Ferroelectr.* **2001**, *33*, 235.
(22) Chattopadhyay, S.; Kvit, A.; Kumar, D.; Sharma, A. K.; Sankar, J.; Narayan, J.; Knight, V. S.; Coleman, T. S.; Lee, C. B. *Appl. Phys. Lett.* **2001**, *78*, 3514.
(23) Lee, H. N.; Zakharov, D. N.; Senz, S.; Pignolet, A.; Hesse, D. *Appl. Phys. Lett.* **2001**, *79*, 2961.
(24) Liu, X. H.; Liu, Z. G.; Liu, J. M. *Appl. Phys. A: Mater. Sci. Process.* **2001**, *73*, 331.
(25) Karasawa, J.; Hamada, Y.; Ohashi, K.; Natori, E.; Oguchi, K.; Shimoda, T.; Joshi, V.; McMillan, L. D.; Paz de Araujo, C. A. *Integr. Ferroelectr.* **2001**, *39*, 1149.
(26) Zhu, T.; Wang, Y. P.; Zhou, L.; Liu, Z. G. *Mater. Sci. Eng. B* **2002**, *89*, 390.
(27) Sugiyama, H.; Kodama, K.; Nakaiso, T.; Noda, M.; Okuyama, M. *Integr. Ferroelectr.* **2001**, *34*, 81.
(28) Lee, K. S.; Sohn, D. S.; Hong, S. H.; Lee, W. I.; Kim, Y. T.; Chae, H. K.; Chung, I. *Thin Solid Films* **2001**, *394*, 142.
(29) Wang, W.; Zhou, Y.; Chen, S.; Ye, F.; Jia, D. *J. Mater. Sci. Technol.* **2001**, *17*, 25.
(30) Li, A.-D.; Wu, D.; Ling, H.-Q.; Wang, M.; Liu, Z.; Ming, N. *J. Cryst. Growth* **2002**, *235*, 394.
(31) Tejedor, P.; Ocal, C.; Barrena, E.; Jimenez, R.; Alemany, C.; Mendiola, J. *J. Electrochem. Soc.* **2002**, *149*, F4.
(32) Ling, H.; Li, A.; Wu, D.; Yu, T.; Zhu, X.; Yin, X.; Wang, M.; Liu, Z.; Ming, N. *Integr. Ferroelectr.* **2001**, *33*, 253.
(33) Ogata, N.; Nagata, M. *Jpn. J. Appl. Phys., Part 1* **2001**, *40*, 2403.
(34) Calzada, M. L.; Gonzalez, A.; Jimenez, R.; Alemany, C.; Mendiola, J. *J. Eur. Ceram. Soc.* **2001**, *21*, 1517.

10.1021/cm021190a CCC: $22.00
Published on Web 10/03/2002

β-Diketonate precursors are widely used for Sr-related MOCVD processes, and in particular, the second-generation $Sr(hfac)_2$tetraglyme (H-hfac = 1,1,1,5,5,5-hexafluoroacetylacetone) precursor has proved to be an efficient source for MOCVD processes[1,44] including routes to SBT.[43]

Despite the fact that a lot of work has been carried out, many questions associated with the subtle interplay between the film quality and mechanicistic aspects of the thermally activated precursor decomposition still remain largely unresolved. There is no doubt, however, that high-quality Sr-containing films require an accurate tuning of factors which govern the growth processes under various operating conditions.

In this perspective, the present paper reports on the behavior of the second-generation $Sr(hfac)_2$tetraglyme precursor in MOCVD processes. This study combines "in situ" FTIR analysis and "ex situ" probing of chemical, structural, and morphological properties of deposited films. Attention has been focused on the interplay among process parameters, deposition mechanism, and film properties. The effects of reactor geometry, temperature of the substrate, reacting/carrier gas composition, and precursor partial pressure have also been addressed.

Experimental Section

Experiments were performed in reduced pressure, horizontal cold wall and hot wall reactors.

The cold wall reactor was a multicomponent, horizontal, MOCVD reactor made of an 80-cm-length quartz tube (i.d. = 8 cm). The reactor consisted of contiguous sections, independently heated within ±2 °C, using computer-controlled hardware, for precursor sublimation/evaporation, gas mixing, and film deposition. Films were deposited on substrates placed on the susceptor (Advanced Ceramics Boralectric Heating Element) similarly independently heated. The reactor was evacuated with a single-stage EDWARDS rotary pump. The total pressure and flow rates were controlled using an EDWARDS ASG 1000 mbar gauge, an adjustable EDWARDS "Speedivalve", and Brooks mass flow controllers.

The hot wall MOCVD reactor consisted of a quartz tube (40-cm length, 2.4-cm i.d.) with an external stainless steel evaporator. The deposition zone was resistively heated with an external ceramic element (15-cm length). The "in situ" FTIR apparatus basically consisted of a MOCVD hot wall reactor with both a perpendicular gas inlet and gas outlet (relative to the reactor longitudinal axis) and an external stainless steel evaporator, interfaced with a 4600/ FT/IR 430 Jasco spectrometer. A detailed description of the experimental apparatus is reported elsewhere.[44]

In the hot wall reactor, the temperatures of the evaporator, connecting lines, and reaction zones were controlled by EUROTHERMS Controls 2132 and 2216. Connecting lines (stainless steal) were always held at slightly higher temperatures than the evaporator to prevent vapor condensation. Flow rates were controlled (within ±2 sccm) using MKS flow controllers and a MKS controller type 247 four-channel read out. Reactors were evacuated by single-stage EDWARDS rotary pumps. The total pressure was controlled using an EDWARDS ASG 1000-mbar gauge, an EDWARDS AGC controller and an adjustable EDWARDS "Speedivalve".

In the typical MOCVD experiments under oxidizing conditions, O_2 (99.999%) was flown (500 sccm) directly into the deposition chamber as reaction gas. Prepurified Ar (99.999%) was used as the carrier gas (100 sccm) to transport the precursor under an inert atmosphere throughout the evaporator into the deposition zone. The overall result was a Ar/O_2 (1:5) mixture in the reaction chamber.

Experiments performed under pure Ar use Ar both as a carrier gas (100 sccm) and for inert gas flow (500 sccm).

$Sr(hfac)_2$ tetraglyme was synthesized from $Sr(OH)_2 \cdot 8H_2O$ (STREM chemicals Inc.) and Hhfac and tetraglyme (Aldrich) according to the literature.[45] Briefly, $Sr(OH)_2 \cdot 8H_2O$ (11.8 mmol) was first suspended in toluene, and then tetraglyme (11.3 mmol) was added to the suspension. Hhfac (22.6 mmol) was added under stirring after 5 min and the mixture was refluxed for 1 h. After the excess hydroxide was filtered off and the water phase was separated from the organic layer containing the adduct, the clear solution was evaporated in vacuo. The obtained solid was crystalizated in pentane. Elemental microanalysis, IR spectra, and TGA curves showing a single sublimation step were in good agreement with reported data for pure $Sr(hfac)_2$ tetraglyme.[45] It is important to note that chemical and thermal properties of the precursor remain identical after several sublimation cycles in vacuo, thus proving adduct stability during sublimation.[45]

Films were deposited on $Pt/TiO_2/SiO_2/Si$ substrates heated in the 250−500 °C temperature range under a total pressure of 6 Torr. The sublimation temperatures of precursor were in the 100−150 °C range.

In all experiments the total quantity of the sublimed precursor was determined by weight loss measurements.

IR spectra of the vapors during MOCVD processes were recorded in the 4500−700 cm^{-1} spectral region.

X-ray photoelectron spectroscopy (XPS) measurements were performed with a PHI 5600 Multy Technique System equipped with an Al standard X-ray source operating at 14 kV and a hemispherical analyzer. The electron takeoff angle (θ) was 45°. Depth profiles were obtained by alternating sputter etching rastered over a 3 × 3 mm area, (with a 4-kV argon ion gun) and XPS analysis. B.E. data were calibrated on C 1s at 285 eV.[46,47] The sputtering rate of SrF_2 films was estimated on standard SrF_2 films whose thickness was determined by SEM cross sections.

Grazing angle XRD measurements (GXRD) were made with a Bruker AXS D5005 X-ray diffractometer equipped with a copper anode and an attachment for thin film measurements. $20° < 2\theta < 70°$ detector scans were adopted. The angle between the X-ray source and the sample surface was fixed at 2°.

Scanning electron microscopy (SEM) was performed with a LEO 1400 Microscope equipped with EDX windowless microanalysis that allows analysis of light elements up to Be.

Growth rates were estimated from EDX data and SEM cross sections.

Carbon contamination has been estimated by XPS depth profiles and EDX microanalysis. Calibration has adopted carbon-containing compounds ($Sr(hfac)_2$ tetraglyme, $Sr(hfac)_2$, $Sr(CH_3COO)_2$), and SrF_2 as references.

(35) Hironaka, K.; Isobe, C.; Moon, B.-K.; Hishikawa, S. *Jpn. J. Appl. Phys., Part 1* **2001**, *40*, 680.
(36) Saito, K.; Ishikawa, K.; Saiki, A.; Yamaji, I.; Akai, T.; Funakubo, H. *Integr. Ferroelectr.* **2001**, *33*, 59.
(37) Moon, B. K.; Hironaka, K.; Isobe, C.; Hishikawa, S. *J. Appl. Phys.* **2001**, *89*, 6370.
(38) Shin, W.-C.; Yoon, S.-G. *Appl. Phys. Lett.* **2001**, *79*, 1519.
(39) Nukaga, N.; Mitsuya, M.; Suzuki, T.; Nishi, Y.; Fujimoto, M.; Funakubo, H. *Jpn. J. Appl. Phys., Part 1* **2001**, *40*, 5595.
(40) Shin, W.-C.; Yoon, S.-G. *J. Electrochem. Soc.* **2001**, *148*, C762.
(41) Bachhofer, H.; Reisinger, H.; Steinlesberger, G.; Schroeder, H.; Nagel, N.; Mikolajick, T.; Cerva, H.; Von Philipsborn, H.; Waser, R. *Integr. Ferroelectr.* **2001**, *39*, 1139.
(42) Kang, S.-W.; Yang, K.-J.; Yong, K.-J.; Rhee, S.-W. *J. Electrochem. Soc.* **2002**, *149*, C44.
(43) Baeri, A.; Condorelli, G. G.; Fragalà, I. L. *Mater. Res. Symp. Proc.* **2001**, *655*, CC5.5.1.
(44) Condorelli, G. G.; Gennaro, S.; Fragalà, I. L. *Chem. Vap. Deposition* **2000**, *6*, 185.
(45) Malandrino, G.; Castelli, F.; Fragalà I. L. *Inorg. Chim. Acta* **1994**, *224*, 203.
(46) Teterin, Y. A.; Sosulnikov, M. I. *Physica C* **1993**, *212*, 306.
(47) Swift, P. *Surf. Interface Anal.* **1982**, *4*, 47.

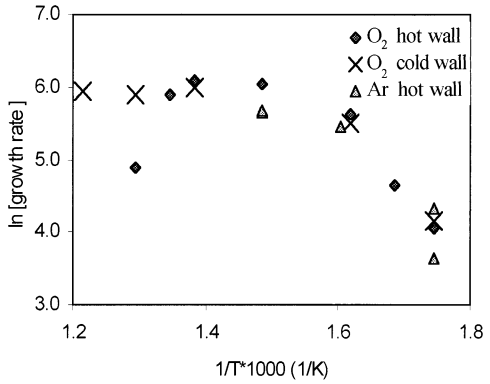

Figure 1. Growth rate dependence upon temperature under various experimental conditions: (◆) hot wall reactor under Ar/O_2; (×) cold wall reactor under Ar/O_2; (▲) hot wall reactor under pure Ar.

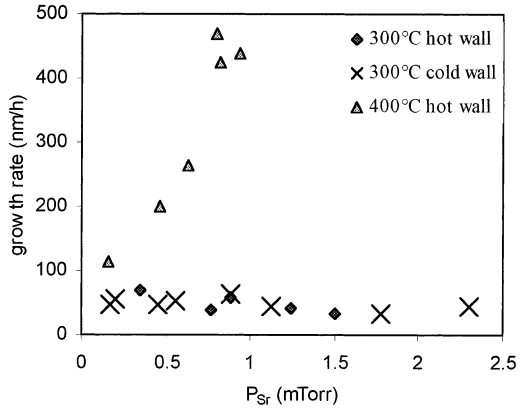

Figure 2. Growth rate dependence upon Sr partial pressure (P_{Sr}) under Ar/O_2: (◆) hot wall reactor at 300 °C; (×) cold wall reactor at 300 °C; (▲) hot wall reactor at 400 °C.

Results and Discussion

Chemical Nature of Films. Typical MOCVD experiments adopting Ar/O_2 mixtures (100/500 sccm) result in the formation of randomly oriented SrF_2 films throughout the investigated deposition temperature range (250−500 °C).

It is generally observed that, in the investigated temperature range (250−500 °C), films consist of randomly oriented SrF_2. GXRD patterns of typical films deposited at 300 and 500 °C showed, in both cases, the (111), (220) and (311) SrF_2 reflections and those of Pt (111) and (200) due to the Pt substrate.

The integrity of SrF_2 films was studied by XPS measurements. In all cases, the binding energy (B.E.) values of the Sr 3d spin−orbit doublet ($3d_{3/2}$ 133.9 eV and Sr $3d_{5/2}$ 135.6 eV) point to SrF_2.[48] Similarly, the B.E. of the F 1s peak (684.9 eV) is consistent with SrF_2.[48] Note that a secondary peak at 688.8 eV is observed in films deposited below 400 °C. This feature can be assigned to chemisorbed ligand fragments containing CF_x groups.[48,49] After sputtering, this band is no longer detectable, thus indicating the presence of SrF_2 in the bulk of the films. Carbon and oxygen photoemission features (at 285 and 532 eV, respectively) are due to surface contaminants. After Ar^+ ion sputtering, no significant carbon and oxygen contaminations were observed (<3%).

Some complementary experiments were performed under pure Ar to understand the role of oxygen in the deposition process. GXRD patterns of films deposited under pure Ar are similarly consistent with polycrystalline SrF_2. XPS spectra, however, have shown relevant carbon contaminations in the bulk, likely due to ligand fragments trapped in the growing films.

The carbon atomic concentration was about 10% in films deposited at 300 °C and it grows up to 20% at 400 °C.

Deposition Kinetics. Growth rates depend on both deposition/substrate temperature (T) and precursor partial pressure (P_{Sr}). Trends are similar in hot and cold wall reactors (Figures1 and 2). The log plot of the dependence of the deposition rate vs $1/T$ is linear, for P_{Sr} = 0.8 mTorr, below 350 °C, thus indicating a reaction-rate-limited process (Figure 1). The apparent activation energy is 100 ± 20 kJ/mol. In the 350−450 °C range the rate remains almost constant (mass-transport rate-limited regime). Beyond 450 °C a remarkable falloff is observed in the hot wall reactor due to precursor depletion either on the reactor wall or in the gas phase, whereas the rate remains constant in the cold wall reactor since precursor depletion is precluded.

Under pure Ar, growth rates have similar trends (Figure 1), thus demonstrating that O_2 does not affect growth kinetics, while precluding the carbon contamination.

The effects of P_{Sr} upon the growth rate have been investigated at various temperatures. Experiments carried out at T = 400 °C (mass-transport rate-limited regime) show (Figure 2) that the deposition rate depends linearly on P_{Sr} in the investigated 0.1−2 mTorr range.

At T = 300 °C, hence, under the reaction-rate-limited regime, the deposition rate does not depend on P_{Sr} in the 0.1−2.3 mTorr range (Figure 2), thus indicating a zero-order kinetics relative to the precursor concentration. This behavior points to a surface reaction where the active sites are saturated for all the investigated partial pressures. Deposition processes controlled by the reaction rate show similar kinetics both in hot wall and in cold wall reactors. It, therefore, transpires that under reaction-rate-limited regimes processes are driven by physical and chemical parameters (gas composition, temperature, reagent residence times, and partial pressures) with no influence due to the reactor geometry. This observation is clearly of relevance in the perspective of scaled reactors for industrial applications.

Gas Phase "in Situ" Analyses. Hints of the deposition mechanism can be obtained from the study of the decomposition process involving the precursor in the vapor phase. Gas-phase compositions, depending upon the reactor temperatures, have been investigated "in situ" in the hot wall reactor equipped for FTIR measurements.

The precursor IR modes associated with the $C-F_x$ stretches (1255−1220 cm^{-1}), the C=C/C=O stretches at 1660 cm^{-1}, and the $C-H_x$ stretches in the 2950−2850 cm^{-1} region[44,50] have been used to monitor the precursor

(48) Moulder, J. F.; Stickle, W. F.; Sobol, P. E.; Bomben, K. D. In *Handbook of X-ray Photoelectron Spectroscopy*; Chastain, J., Ed.; Perkin-Elmer Corporation, Physical Electronic Division, Eden Praire, Minnesota, 1992.

(49) Lagutchev, A. S.; Song, K. J.; Huang, J. Y.; Yang, P. K.; Chuang, T. J. *Chem. Phys.* **1998**, *226*, 337.

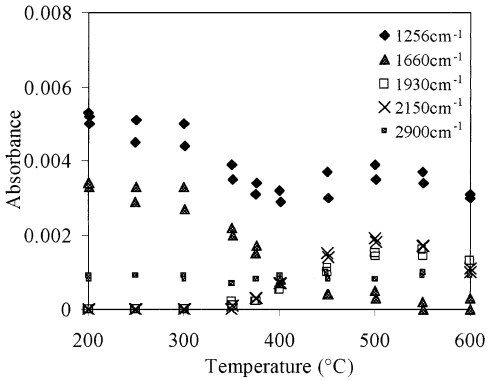

Figure 3. Dependence of the absorbance of relevant IR bands vs T (°C) in MOCVD processes in an Ar/O_2 enviroment: (◆) 1256 cm^{-1} ($Sr(hfac)_2$ tetraglyme, C−F stretch); (▲) 1660 cm^{-1} ($Sr(hfac)_2$ tetraglyme, C═O/C═C stretches); (□) 1930 cm^{-1} (carbonyls such as CF_2O); (×) 2150 cm^{-1} (C═C═O stretch, acylketenes); (■) 2900 cm^{-1} (C−H stretches, tetraglyme).

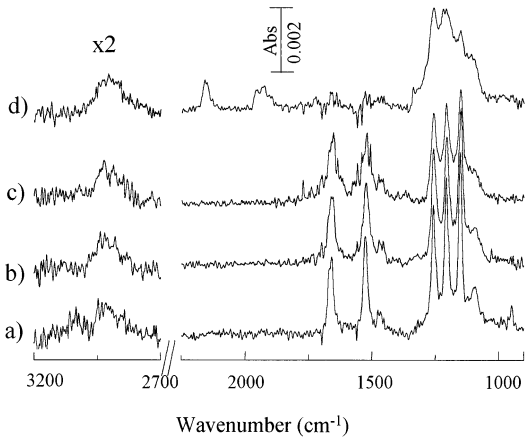

Figure 4. "In situ" IR spectra of $Sr(hfac)_2$ tetraglyme at various reactor temperatures and gas compositions in an Ar/O_2 enviroment: (a) $T = 200$ °C; (b) $T = 300$ °C; (c) $T = 350$ °C; (d) $T = 450$ °C.

concentration in the gas phase. The absorbance value associated with each vibration has been calculated as [$\log(I_0/I)$] where I_0 is the background intensity and I the peak intensity.

Absorbance dependencies upon temperature and typical spectra are shown in Figures 3 and 4, respectively.

Up to 300 °C the spectra do not show changes in both the absorbance values and the band shapes. (Figures 3 and 4a,b), thus indicating constant gas-phase compositions. This observation points unambiguously to no decomposition in the gas phase. Film deposition at 300 °C, therefore, simply involves the adsorption of intact precursor followed by decomposition to SrF_2. Note that under reaction-rate-limited regimes, the precursor consumption on the surface is balanced by the feed rate and, therefore, the gas-phase concentration does not change.

Upon increasing the temperature (350 °C), all the bands at 1255−1220 cm^{-1} (C−F_x stretches) and 1660 cm^{-1} (C═C/C═O stretches) associated with the hfac framework decrease in intensities (Figure 3), while maintaining the same shape (Figure 4c). This effect can

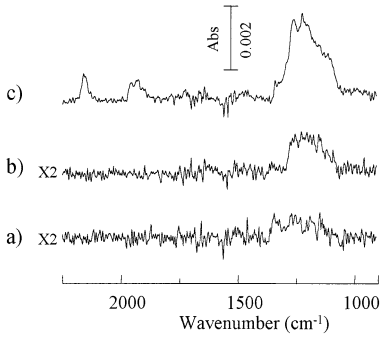

Figure 5. IR difference spectra of $Sr(hfac)_2$ tetraglyme at various reactor temperatures: (a) 300 °C minus 200 °C; (b) 350 °C minus 200 °C; (c) 450 °C minus 200 °C.

be due to the thermal enhancement of the surface reactions and, in turn, to the faster (than feeding) consumption of the precursor. By contrast, modes at 2950−2850 cm^{-1} (C−H_x stretches) do not show any intensity falloff. These modes are associated with the tetraglyme either coordinated to the metal center or free.[44] Thus, the observed trend of relative intensities of C−H_x stretches vs hfac bands is tuned well with a surface process:

$$Sr(hfac)_2 \text{ tetraglyme (g)} \rightarrow Sr(hfac)_2 \text{ (ad)} + \text{tetraglyme (g)} \quad (1)$$

Note in this context that the expected C−O stretches of the free glyme (at 1125 cm^{-1}) are not clearly seen since they are hidden by the more intense C−F_x stretches that fall in the same region. The disappearance, however, of the valley around 1120 cm^{-1} (Figure 4c) in the spectra recorded at 350 °C seems compatible with the presence of these modes.

Information on the nature of other decomposition products can be gained from the differential absorbance spectra obtained (Figure 5) upon subtracting absorbances of the intact precursor at 200 °C from values taken from IR spectra at various temperatures. At 300 °C (Figure 5a) absorbances due to decomposition byproducts are too weak to be clearly detected. At 350 °C (Figure 5b), a broad band between 1300 and 1000 cm^{-1} (hence, in the spectral region of C−F_x stretches) becomes apparent and this feature can be associated with fluorocarbon species desorbing from the surface of the growing film.

Above 375 °C, all the IR spectra show much more complex features due to decomposition processes. Absorptions due to C═O/C═C stretches of the precursor ring are considerably less intense (Figures 3 and 4d), while those due to C−F_x stretches still remain evident but with changed shapes (Figures 3 and 4d). By contrast, the intensity of the band due to C−H_x stretches of the tetraglyme appears unchanged (Figures 3 and 4d). These observations suggest new precursor decomposition pathways either in the gas phase or on the surface, involving the breakdown of the β-diketonate ring and leading to new fluorinated products responsible for the C−F_x stretches still present. Moreover, two new peaks become evident at 1930 and 2150 cm^{-1}. The band at 2150 cm^{-1} falls in the spectral region of the stretch of

(50) Lin-Vien, D.; Colthup, N. B.; Fateley, W. G.; Grasselli, J. G. *The Handbook of Infrared and Raman Characteristic Fraquencies of Organic Molecules*; Academic Press: San Diego, 1991; p 213.

the carbon monoxide,[51] but it has a different shape since it lacks the P and R branches generally detectable in the spectrum of CO. The position and the shape of this peak are, however, consistent with the stretches of ketenes or acylketenes, >C=C=O.[50,52] Carbonyls such as CF_2O can be associated with the broad envelope around 1930 cm^{-1}. Previous studies of MOCVD decomposition routes for both Hhfac and La(hfac)$_3$diglyme have already pointed out[44] that trifluoroacylketene and carbonyls (probably CF_2O) are responsible for IR features around 2150 and 1930 cm^{-1}, respectively. Acylketene species are also formed as byproducts of the pyrolysis of β-keto esters at 400−900 °C[53] as well as in the decomposition pathways of various metal β-diketonates.[54−57]

To evaluate the heterogeneous vs homogeneous nature of this high-temperature pathway, the dependence of gas composition on temperature has been investigated in the presence of a metallic surface (Al) around the inner walls of the reactor. It was found that the more reactive surface enhances the rate of the heterogeneous reaction; in fact, the FT-IR absorbances associated with the 1255−1220 and 1660 cm^{-1} precursor bands begin to decrease in intensity at lower temperature (250 °C) with respect to the experiments performed without the metallic surface, reported above. Moreover, the nature of the high-temperature (above 400 °C) byproducts, acylketenes (2150 cm^{-1}) and CF_2O (1950 cm^{-1}), remains unchanged, even though their intensities are lower than those obtained without the metallic surface. This behavior suggests that beyond 400 °C precursor decomposition occurs in the gas phase since the reaction pathway is not surface-dependent. The rate, however, decreases due to the enhancement of the competing heterogeneous reaction.

Note that the observed high-temperature decomposition can be responsible for the precursor depletion in the hot wall reactors and, hence, for the growth rate falloff above 450 °C.

In the absence of oxygen the temperature dependence of absorbances of relevant IR bands (Figure 6) do not show any change up to 300 °C, similar to processes under Ar/O_2. Above this temperature, the characteristic IR features of the Sr(hfac)$_2$ tetraglyme precursor (C=C/C=O stretches and CF_x stretches) undergo a sizable intensity decrease. By contrast (and similar to Ar/O_2 experiments) the intensity of tetraglyme CH_x stretches remains constant, thus suggesting the same ligand dissociation and generation of the free not-decomposed glyme. Above 400 °C decomposition processes lead to the formation of new fluorinate species. It is interesting

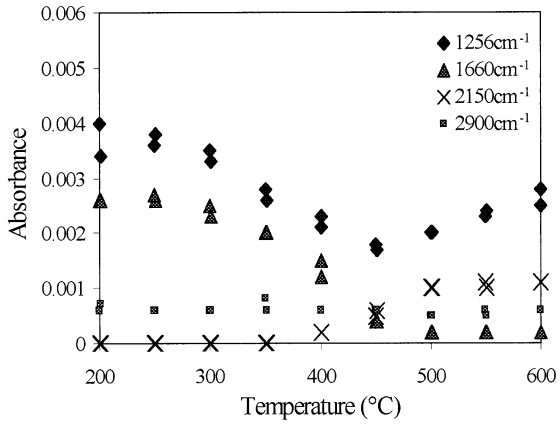

Figure 6. Dependence of the absorbance of relevant IR bands vs *T* (°C) in MOCVD processes in a pure Ar environment: (◆) 1256 cm^{-1} (Sr(hfac)$_2$ tetraglyme, C−F stretch); (▲) 1660 cm^{-1} (Sr(hfac)$_2$ tetraglyme, C=O/C=C stretches); (×) 2150 cm^{-1} (C=C=O stretch, acylketenes); (■) 2900 cm^{-1} (C−H_x stretches, tetraglyme).

Chart 1

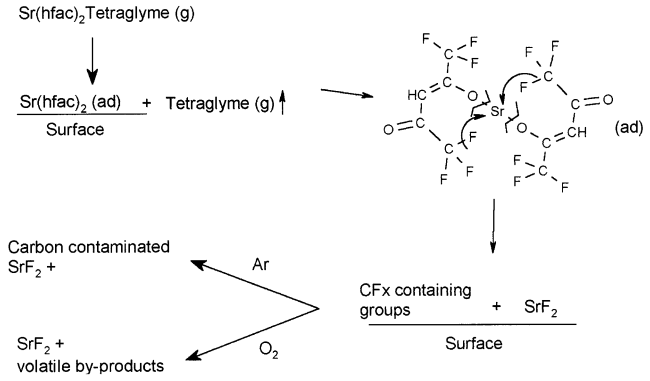

to note that under pure Ar the fluorinate ketene at 2150 cm^{-1} is the main decomposition product, while CF_2O, responsible for IR features at 1930 cm^{-1} observed under oxygen, is no longer present.

Reaction Mechanisms. On the basis of the results described above, it becomes possible to propose qualitative mechanisms governing the MOCVD decomposition of Sr(hfac)$_2$ tetraglyme. Below 350 °C, precursor does not decompose in the gas phase and the deposition pathway involves the adsorption of the precursor on the film surface. This is consistent with no evidence being found for gas-phase decomposition processes in FT-IR experiments and with the growth rate dependence upon P_{Sr} (Figure 1). Adsorption probably causes the glyme dissociation according to eq 1. Further surface reactions lead to the fluorine transfer to the metal followed by the demolition of the β-diketonate framework (Chart 1). Alternative pathways, however, involving first dissociation of CF_x-containing groups, followed by fluorine transfer from the CF_x moiety to the metal, cannot be ruled out. The overall result is the formation of the SrF_2 film and of the adsorbed CF_x-containing species, consistent with the XPS data and IR analysis of desorbed species as well as with data reported for surface decomposition of closely related species.[58−60] Consistent

(51) Nyquist, R. A. *The Interpretation of Vapor-Phase Infrared Spectra*, Vol. 1; Stadtler Research Laboratories: Philadelphia, 1984; p 9.
(52) Moore C. B.; Pimentel, G. C. *J. Chem. Phys.* **1963**, *38*, 2816.
(53) Freiermuth, B.; Wentrup C. *J. Org. Chem.* **1991**, *56*, 2286.
(54) Turgambaeva, A. E.; Bykov A. F.; Igumenov, I. K. *J. Phys. IV* **1995**, *C5*, 221.
(55) Bykov, A. F.; Turgambaeva, A. E.; Igumenov I. K.; Semyannikov, P. P. *J. Phys. IV* **1995**, *C5*, 191.
(56) Turgambaeva, A. E.; Krisyuk, V. V.; Bykov A. F.; Igumenov, I. K. *J. Phys. IV* **1999**, *Pr8*, 65.
(57) Condorelli, G. G.; Hitchman, M. L.; Kovalgin, A. Y.; Shamlian, S. H. In *Chemical Vapor Deposition—Proceedings of the Fourteenth International Conference and EUROCVD-11*; Allendorf, M. D., Bernard, C., Eds; The Electrochemical Society: Pennington, NJ, 1997; Vol. 97-25, p 901.
(58) Girolami, G. S.; Jeffries, P. M.; Dubois, L. H. *J. Am. Chem. Soc.* **1993**, *115*, 1015.
(59) Parmeter, J. E. *J. Phys. Chem.* **1993**, *97*, 11530.

Chart 2

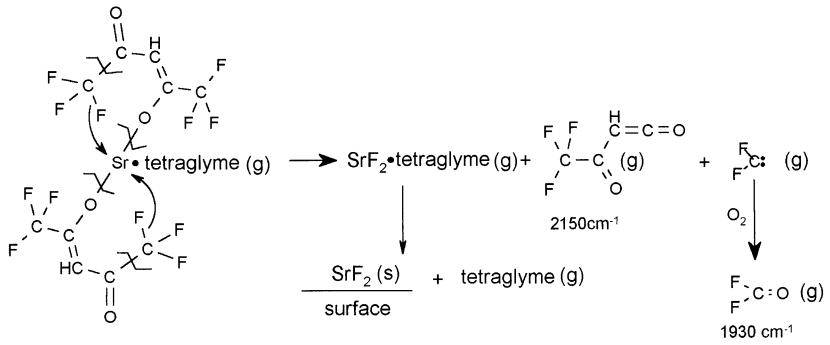

with the kinetics of experiments under Ar, there is evidence that the oxygen does not play a crucial role in the SrF_2 formation. Indeed, O_2 is needed only to preclude carbon contaminations in the films since it governs oxidation of surface species.

At temperatures beyond 400 °C a homogeneous decomposition pathway of $Sr(hfac)_2$ tetraglyme becomes relevant. This pathway probably involves intramolecular fluorine transfer from carbon to Sr through the switching from bidentate to monodentate of the ligand coordination. The thermally activated opening of the chelate ring is not an unexpected issue since it has been proposed for closely related systems.[56,61,62] The proposed pathway (Chart 2) finally leads to the SrF_2 deposition and to the production of CF_2O (in the presence of oxygen) and fluoroacylketens.

Conclusions

The MOCVD process for SrF_2 film growth from $Sr(hfac)_2$tetraglyme precursor was studied in hot wall and cold wall reactors. Depending on operational conditions, the process involves two different deposition regimes: reaction-rate-limited and mass-transport rate-limited regimes. Depositions governed by reaction-rate-limited regimes do not depend on the geometrical reactor configuration. This observation is of relevance to extrapolate kinetic and mechanistic studies in reactors for industrial applications. The study of the kinetics of SrF_2 deposition, combined with "in situ" FTIR and "ex situ" XPS analyses of both the gas phase and of the SrF_2 films, has provided crucial information on reaction pathways involved in the $Sr(hfac)_2$ tetraglyme decomposition. At low temperature (<350 °C), a heterogeneous mechanism based on the precursor adsorption followed by the demolition of the β-diketonate framework is operating. Oxygen is not involved in the rate-determinant steps, but it plays an important role in preventing carbon contaminations. At higher temperatures (>375 °C) a homogeneous decomposition pathway, leading to fluoroacylketenes and CF_2O, accompanies SrF_2 film growth. To conclude, the present study of mechanisms that drive the SrF_2 film formation is of relevance for optimizing the deposition of single-component films, but even more importantly, it becomes a useful tool for the design of novel MOCVD routes for more complex, multicomponent Sr-containing films.

Acknowledgment. We gratefully thank the European Commission (IST-2000-30153-FLEUR contract) for financial support.

Supporting Information Available: GXRD patterns and XPS spectra of SrF_2 films deposited at 300 and 500 °C (PDF). This material is available free of charge via the Internet at http://pubs.acs.org.

CM021190A

(60) Lin, W.; Wiegand, B. C.; Nuzzo, R. G.; Girolami, G. S. *J. Am. Chem. Soc.* **1996**, *118*, 5977.
(61) Pollard, K. D.; Jenkins, H. A.; Puddephatt, R. J. *Chem. Mater.* **2000**, *12*, 701.
(62) Harima, H.; Ohnishi, H.; Hanaoka, K.; Tachibana, K.; Kobayashi, M.; Hoshinouchi, S. Jpn. *J. Appl. Phys.* **1990**, *29*, 1932.